

Experimental assessment of the energy performance of microfluidic glazing components: The first results of a monitoring campaign carried out in an outdoor test facility

*Original*

Experimental assessment of the energy performance of microfluidic glazing components: The first results of a monitoring campaign carried out in an outdoor test facility / Baracani, Manuela; Favoino, Fabio; Fantucci, Stefano; Serra, Valentina; Perino, Marco; Introna, Marisandra; Limbach, Rene; Wondraczek, Lothar. - In: ENERGY. - ISSN 0360-5442. - ELETTRONICO. - 280:(2023), p. 128052. [10.1016/j.energy.2023.128052]

*Availability:*

This version is available at: 11583/2979582 since: 2023-06-26T10:40:55Z

*Publisher:*

elsevier

*Published*

DOI:10.1016/j.energy.2023.128052

*Terms of use:*

This article is made available under terms and conditions as specified in the corresponding bibliographic description in the repository

*Publisher copyright*

(Article begins on next page)



# Experimental assessment of the energy performance of microfluidic glazing components: The first results of a monitoring campaign carried out in an outdoor test facility

Manuela Baracani<sup>a,\*</sup>, Fabio Favoino<sup>a</sup>, Stefano Fantucci<sup>a</sup>, Valentina Serra<sup>a</sup>, Marco Perino<sup>a</sup>, Marisandra Introna<sup>a</sup>, Rene Limbach<sup>b,c</sup>, Lothar Wondraczek<sup>b,c</sup>

<sup>a</sup> TEBE Research Group, Department of Energy, Politecnico di Torino, Corso Duca Degli Abruzzi, 24, 10129, Turin, Italy

<sup>b</sup> Otto Schott Institute of Materials Research, University of Jena, Fraunhoferstrasse 6, 07743, Jena, Germany

<sup>c</sup> Center of Energy and Environmental Chemistry – CEEC, Jena, University of Jena, Philosophenweg 7a, 07743, Jena, Germany

## ARTICLE INFO

Handling Editor: Neven Duic

### Keywords:

Adaptive façades  
Advanced fenestration systems  
Smart windows  
Water-flow glazing  
Building energy efficiency

## ABSTRACT

Microfluidic glazing is a newly developed, adaptive, transparent component characterized by micro-channels filled with a circulating liquid, functioning as a heat exchanger and controlling the heat transfer through a façade. The performance of this glazing depends on its design and operation on site. The aim of this study is to present the results of an in-situ performance evaluation of microfluidic glazing components obtained from an experimental campaign in outdoor test cells, and to explore their potential and limitations under realistic working conditions. A case study has been conducted in Turin, Italy, in which two small south-oriented triple glazing units, upgraded with different functional elements, including a laminated semi-transparent Perovskite solar cell and microfluidic glazing, have been investigated under different operating conditions. Overall, the experimental campaign has shown a reduction in the heat exchange through the façade of about 70%. Moreover, this technology allows the temperature in the Perovskite solar cell to be decreased by as much as 10 °C, and the central glazing temperature to be reduced by as much as 41 °C, when set as the central panel, thereby effectively decreasing the risk of thermal degradation or thermal shocks. A temperature difference of 12 °C and 16 °C was recorded, depending on the modules, between the inlet and outlet temperatures.

## 1. Introduction

Climate change and the increase in energy consumption have led worldwide economies to set up carbon neutrality objectives [1]. As the building sector is responsible for a large part of the world's energy demand [2], the reduction of building energy use, while maintaining the occupants' well-being, has been one of the essential targets of the latest research [3]. Transparent elements in the façade of a building play a central role in controlling the energy consumption and ensuring the users' comfort. In particular, Adaptive Transparent Façades (ATFs), such as dynamic shadings, smart glazing [4], double-skin façades, as well as air- and water-flow windows, can enhance the quality of the indoor environment and reduce the energy consumption by dynamically adapting to the external or internal boundary conditions [5]. Among the various ATFs, Water-Flow Glazing (WFG) is a technology that is able to vary the thermal transmittance ( $U_{\text{value}}$ ) and solar heat gain coefficient

( $g_{\text{value}}$ ), and control the heat transfer through the transparent façade [6]. This technology consists of a glazing element with cavities that are used for the circulation of water, or a hydroalcoholic solution, which is supplied by a pump [7]. The presence of water, a spectrally-selective liquid with a high heat capacity, leads to the absorption of solar radiation in the Far Infrared Region (FIR), while preserving the optical transparency over the Near Infrared (NIR) and Visible (Vis) spectral range [8]. The thermal behavior of the transparent component can be modulated based on the control of the temperature and flow rate of the circulating liquid without its optical properties being affected [6]. WFG can be utilized in different ways, depending on its configuration and operating conditions, as explained in Ref. [9]. It can be used as either a cooling or a preheating component, which involves supplying the circulating liquid at a constant temperature, from the water supply network or a large thermal mass source, thereby reducing the heat transfer through the façade and controlling the glazing temperature [10]. WFG can also be used to harvest heat through solar-thermal

\* Corresponding author.

E-mail address: [valentina.serra@polito.it](mailto:valentina.serra@polito.it) (M. Baracani).

<https://doi.org/10.1016/j.energy.2023.128052>

Received 18 January 2023; Received in revised form 12 May 2023; Accepted 6 June 2023

Available online 7 June 2023

0360-5442/© 2023 The Authors. Published by Elsevier Ltd. This is an open access article under the CC BY-NC-ND license (<http://creativecommons.org/licenses/by-nc-nd/4.0/>).

**Nomenclature**

$AERR$	absolute error
$g_{value}$	solar heat gain coefficient
$g_{value,exp}$	experimental solar heat gain coefficient
$h_e$	external heat transfer coefficient
$h_i$	internal heat transfer coefficient
$I_{en}$	transmitted vertical solar radiation
$I_{hor}$	horizontal global solar radiation
$I_{inc}$	incident vertical solar radiation
$\Lambda$	thermal conductance
$Q_{surf}$	heat flow measured by heat flux meter

$R_{surf,in}$	internal surface resistance
$R_{surf,out}$	external surface resistance
$T_{in}$	indoor air temperature
$T_{out}$	outdoor air temperature
$T_{outlet}$	fluid outlet temperature
$T_{sol}$	solar transmittance
$T_{sol,exp}$	experimental solar transmittance
$T_{vis}$	visible transmission
$U_{value}$	thermal transmittance
$U_{value,exp}$	experimental thermal transmittance
$\Delta T_{outlet-inlet, exp}$	fluid outlet-inlet temperature difference

harvesting and hydronic heat exchange, thereby enabling: i) direct preheating of the water when the water system is connected to the domestic hot water or heating system, or ii) heat storage in building components, including water tanks or Phase Change Materials (PCM) [11], for later use in designated periods (as daily heat collection and night re-irradiation). Yamaç and Koca demonstrated how the use of such a technology could positively impact energy consumptions by reducing the daytime and nighttime electrical energy use by 27% and 45%, respectively [12].

Microfluidic Glazings (MFGs) are a novel type of WFG [13], in which the liquid heat reservoir is harnessed through an array of channels embedded directly within the glazing. They consist of a glass sheet (usually soda-lime silicate float glass, but alternative glasses, such as borosilicates and aluminosilicates, have also been employed) which has an array of micro-capillaries that are used for the circulation of the fluid, and this sheet is bonded, using a polymeric interlayer, to a thin covering glass, for example, a chemically strengthened alkali-aluminosilicate glass cover [14]. This technology minimizes the thickness of the liquid layer, thereby reducing the pumping energy, and maximizing the glazing-fluid interface. When integrated with an Insulating Glazing Unit (IGU), a MFG can be used to replace a conventional glazing layer, and it can be utilized for indoor air conditioning or heat harvesting [15]. The liquid harvesting potential can also be enhanced when the technology is coupled with the Suspended Particle Device (SPD) technology: Heiz et al. (2018) demonstrated how this combination of technologies allows around 360 kWh/(y m<sup>2</sup>) of solar thermal energy to be harvested [16]. It has also been demonstrated how the use of an IGU integrated with an MFG is able to reduce the indoor air temperature of a room by as much as 15 °C in the summer period [17]. The use of circulating water, characterized by a high heat transfer convective coefficient, in addition to offering a higher heat capacity, also produces a higher heat exchange between a glazing and a fluid than traditional flowing-air components, and therefore allows the glazing temperature to be efficiently increased or decreased. However, this is an active system in which the hydraulic pump needs to be continuously powered by electricity. Consequently, an optimal use of this technology involves its use in combination with an integrated façade Photovoltaic (PV) system to obtain the double objective of reducing the power supply and reducing the PV layer temperature [18], in order to decrease the risk of overheating and to maintain a good efficiency [19]. Indeed [20] demonstrated how applying a PV layer on an air-flow window maintained lower environment temperatures in summer while increasing the electrical output of 1.2% in comparison to a not ventilated window. Different studies investigated the coupling of PV with water for heat-recovery objectives [21]: made use of circulating water in a transparent aerogel glazing incorporating Fresnel lens, micro-channel heat pipe and thermoelectric generators to recover the waste heat. Perovskite Solar Cells (PVK) represent a PV technology that is suitable for integration with glazing elements that have recently become competitive, thanks to a single-junction cell power conversion efficiency above 25% [22]. The coupling of MFG and PVK technologies

has been investigated in the Powerskin Plus Project [23], which has the aim of developing innovative façade solutions, based on the smart integration of highly-efficient energy components. The project has involved investigating the coupling of a semi-transparent flexible Perovskite solar cell with MFG, and the possibility of integrating PCMs as energy storage components. This would allow an energy efficient system, based on renewable energy sources, to be designed, in which the PV layer powers the pump that supplies the MFG, while the MFG contributes to decreasing the PV temperature, thus increasing the efficiency of the overall system. Moreover, the circulating fluid would allow energy stored in the PCMs to be harvested for later use. Nevertheless, the complexity and high number of coupled conversion processes involved in such a technology make it necessary to investigate the feasibility, the cost-benefit ratio, and the overall efficiency of the process.

Another critical issue associated with this concept is the lack of specific methodologies and Key Performance Indicators (KPIs) for the experimental assessment of MFG components [18]. To the best of the authors' knowledge, only a limited number of reports have dealt with the dynamic behavior of MFG components tested under realistic operating conditions [13,14,16,17], and none of these have focused on the thermal behavior of the component itself, or on its application in combination with a Perovskite PV layer. Moreover, no information is available on the possible glazing temperature reduction that can be attained with this technology, and no studies have presented an experimental assessment of the KPIs related to the heat transfer of the components.

Furthermore, only a few preliminary examples of full-scale application of this technology [14], which is also a frequent problem for WFGs and adaptive façades in general, are available [24]. This has made it necessary to use validated simulation models for the performance assessment of such a technology. However, at the moment, the only available tool through which it is possible to model and dynamically simulate MFG is the Finite Element Modeling (FEM) tool. However, this type of modeling is rarely included in building-level simulation workflows and is highly time-consuming. Therefore, it is necessary to simulate these components at a simplified level using models that can be validated with intra-software and experimental data. Moreover, experimental data concerning the KPIs that describe the component under real working conditions result to be an essential information to simulate these technologies.

The aim of this study has been to answer the previously presented critical issues by conducting an experimental assessment of the performances of IGUs that incorporate MFG and a PVK layer, regarding the main component-level KPIs and the methodology followed in the study. The thermal behavior of the components, as regards their temperature, thermal transmittance, solar heat gain coefficients, and solar transmission has been thoroughly assessed under different working conditions to provide useful information for the design, operation, and simulation of the technology for future research. The following objectives were addressed in the present work.

- i) collecting experimental data to validate the models and perform a detailed technology assessment (at a component and façade scale) to optimize the performance of a façade;
- ii) identifying the potentials and critical risks of the investigated technology;
- iii) developing a methodology for the assessment of a full-scale mockup (set-up, measurements, experimentation schedule, KPIs, ...).

Simplified models will be built in the next steps of the experimentation and validated with the collected experimental data.

An experimental campaign was set-up for these purposes and was carried out on different configurations of MFG prototypes. Two small-scale Triple Glazing Units (TGUs), equipped with MFGs, one of which included a laminated PVK layer, were installed in a south-oriented test-cell on the roof of the Politecnico di Torino, Italy, and monitored for three months during the winter season. The design of the mock-ups and selection process, conducted by means of simulations, details about the setting up of the experimental campaign, the preliminary results of the investigated parameters and the experimental assessed KPIs are presented hereafter.

## 2. Materials and methods

The overall methodology to evaluate the performance of MFG systems, by means of experimental measurements, was structured in four steps: i) identifying the driving forces and defining the KPIs; ii) designing the IGUs; iii) setting up the experimental campaign; iv) designing the monitoring campaign and data analysis. Simplified models will be developed in the next phase of the experimentation and validated with the collected data.

### 2.1. Identification of the driving forces and definition of the KPIs

As first step of the design phase, the following driving forces for the operation of the MFG technology were identified: i) surface temperature, which was investigated as an indicator of the heat transfer through the component, of the thermal comfort performance, as well as of the PVK efficiency and the risk of glazing thermal shock; ii) difference in the liquid outlet-inlet temperatures, which was considered as an indicator of the heat storage or water-preheating potential; iii) heat flow through the component, which was regarded as an indicator of the thermal performance of the component.

The preliminary KPIs, selected in accordance with [6], to experimentally assess the thermal performance of the technology, were the thermal transmittance ( $U_{\text{value}}$ ) and the total solar heat gain coefficient ( $g_{\text{value}}$ ). These indicators were calculated from experimental data according to the methodology presented in Ref. [25], and are herein referred to as experimental thermal transmittance ( $U_{\text{value,exp}}$ ), experimental solar heat gain coefficient ( $g_{\text{value,exp}}$ ), and experimental solar transmittance ( $T_{\text{sol,exp}}$ ).

As what concerns simulations,  $U_{\text{value}}$  was calculated from the thermal conductance of the component ( $\Lambda$ ) and from the conventional external and internal surfaces resistances ( $R_{\text{surf,out}}$ ,  $R_{\text{surf,in}}$ ) using Equation (1) [26]. The actual surface resistance values were instead considered for the calculation of  $U_{\text{value,exp}}$ , using the outdoor and indoor air temperatures ( $T_{\text{out}}$ ,  $T_{\text{in}}$ ), and the heat flow measured by a heat flux meter ( $Q_{\text{surf}}$ ) placed on the internal surface.  $U_{\text{value,exp}}$  was assessed during the night period (1:00–5:00 a.m.) to avoid the influence of solar radiation on the results.

$$U_{\text{value}} = (R_{\text{surf,out}} + L^{-1} + R_{\text{surf,in}})^{-1} \quad (1)$$

The  $g_{\text{value,exp}}$  parameter was assessed in situ from the indoor and outdoor air temperatures, internal surface heat flows, and the incident and transmitted vertical solar radiation ( $I_{\text{en}}$ ,  $I_{\text{inc}}$ ), using Equation (2)

[25]. The value of  $T_{\text{sol,exp}}$  was assessed from the incident and transmitted solar radiation via Equation (3) and was discretized by the incident angle.

$$g_{\text{value,exp}} = \frac{\int_{24h} I_{\text{en}} dt + \left[ \int_{24h} Q_{\text{surf}} dt - \int_{24h} [U_{\text{value,exp}} \cdot (T_{\text{out}} - T_{\text{in}})] dt \right]}{\int_{24h} I_{\text{inc}} dt} [-] \quad (2)$$

$$T_{\text{sol,exp}} = \frac{I_{\text{en}}}{I_{\text{inc}}} \left[ - \right] \quad (3)$$

An error analysis of the identified KPIs was performed by means of the propagation of uncertainty method, considering the 95% fractile of the temperature error calculated during the calibration of the thermocouples, and the instrument error declared on the technical sheets for the Heat Fluxes and Irradiance.

### 2.2. Designing the IGUs

The second step in the design of the experimental campaign was dedicated to investigating the coupling of the individual functional layers and to testing their performances by means of simulations. This allowed the most promising IGUs to be tested in situ, as suggested in Ref. [18]. For this purpose, several IGUs with different types of coatings, glazing layers, cavity numbers, and PVK and MFG configurations were simulated under simplified steady-state conditions, while neglecting the effect of fluid circulation, and their  $U_{\text{value}}$ ,  $g_{\text{value}}$ , visible transmission ( $T_{\text{vis}}$ ) and surface temperatures were then compared. The spectral thermo-optical properties of the Perovskite PV layer and of the MFG were characterized by means of a dual-beam spectrophotometer (Cary 5000, Agilent). All the spectra were recorded for wavelengths between 200 nm and 2600 nm at 2 nm step widths, using a depolarized beam and a 5.1° incidence operated in reflectance mode. The spectral data were then imported into an “LBNL Optics6” tool [27] and the integrated properties of the MFG and glazing laminated PV layer were calculated. The latter were then imported into LBNL Window 7.7 [28] to assemble the different IGUs and compare their thermal properties and surfaces temperature when operating under a steady-state condition. This analysis allowed us to identify the two configurations that enable the MFG glazing temperature, and consequently the heat storage potential, to be maximized, while maintaining a high thermal performance and an acceptable visible transmission, whenever the PVK layer is not applied. The different IGU configurations modeled with Window7.7 are schematically illustrated in Fig. 1.

### 2.3. Setting up the experimental campaign

The two best-performing configurations were selected, considering the Window simulation results, for testing in the Box for Evaluation of Innovative Building Envelopes (BEIBI), a south-oriented test cell placed on the roof of the Energy Department at the Politecnico di Torino, Italy. The test cell is 1.58 m long, 1.60 m wide and 1.88 m high; it has a replaceable south-exposed façade that can be equipped with different mock-ups. The other walls and top are sandwich partitions ( $U_{\text{value}} \sim 0.33$  W/m<sup>2</sup>K) insulated with an internal wood layer.

The south façade was equipped with two opaque, insulated, sub-modules and two 0.58 m wide and 0.68 m high transparent TGU prototypes, that included MFG components (Fig. 2). Transparent Sub-Module A (TSMA) – which is equivalent to simulated TGU 5 B in Fig. 1, except for the single internal glazing and the cavity gas – is composed of an external MFG and laminated Perovskite PV layer, two 14 mm air cavities and two single glazing layers with low-e coatings on surfaces 3 and 5 (numbered from the exterior to the interior). The PV layer was not electrically connected and hence not operational. Transparent Sub-Module B (TSMB) – which is equivalent to simulated TGU 2 B in Fig. 1, except for the single internal and external glazing – is composed of an external single glazing with a low-e coating on surface 2,



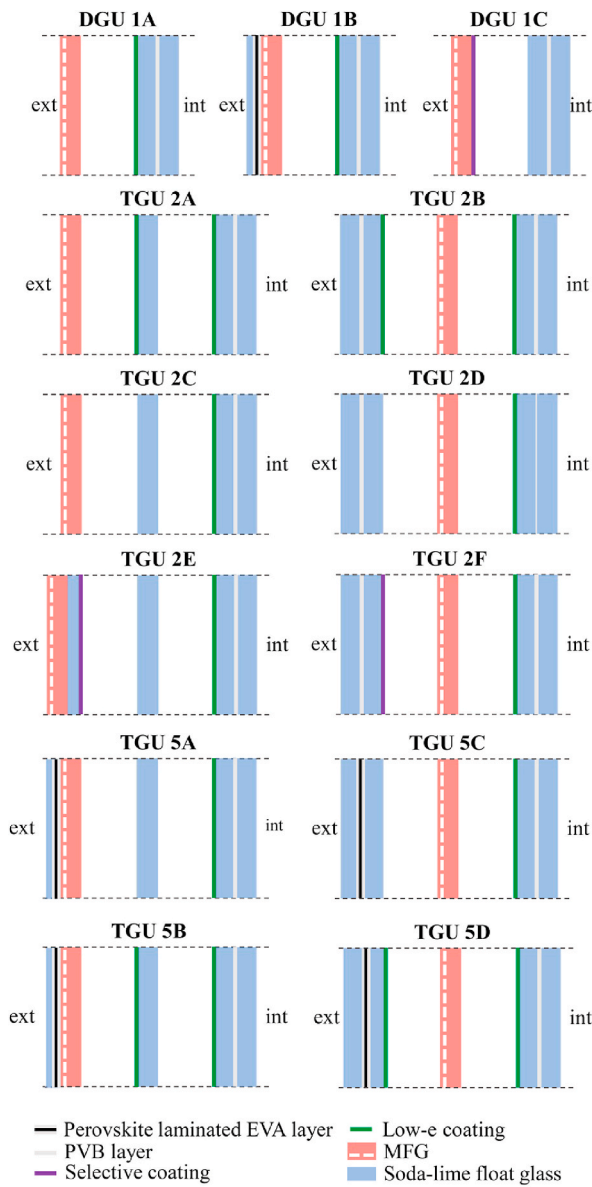


Fig. 1. The IGU configurations analyzed in the LBNL Window. The cavities are filled with an Argon 90%-Air 10% mixture.

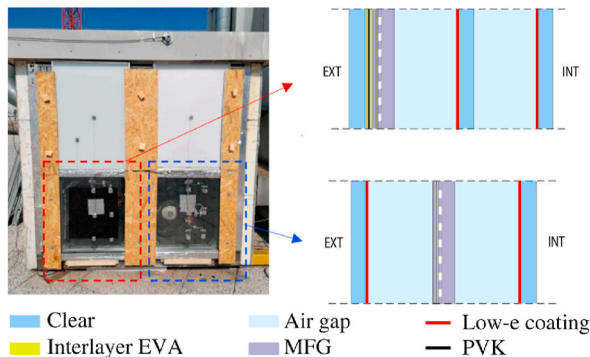


Fig. 2. Experimental test cell and mock-up configurations.

MFG as the central layer and an internal low-e coated (surface 5) single glazing separated by two 14 mm air cavities. The top and bottom of the two MFGs are connected to a steel collector that distributes the liquid to

the horizontal section to enable a homogeneous flow within all the MFG channels [13].

The hydraulic system used to circulate the fluid is described in the following parts and illustrated in Fig. 3. It includes: i) a pumping system (Fig. 4a) in which two submersible water pumps (nominal power of 5 and 8 W, respectively) collect the liquid from a container and distribute it to the MFG components through PVC pipes connected to the distributor at the bottom of the MFG. After circulation through the MFG, the liquid is collected at the top of the MFG and injected, through PVC pipes, into the ii) heat exchanger (Fig. 4b), which consists of PVC pipes immersed in a 300 l water tank, to allow heat to be exchanged between the circulating fluid and the water mass. The tank works as a temperature balancer to keep the inlet temperature of the circulating liquid almost constant; iii) a mixing container, which maintains the inlet temperature for the two mock-ups equal, the liquid – after passing through the heat exchanger – is mixed in the container by the pumping system. In such type of hydraulic system the prevalence of the pump was found as a leading parameter for a proper circulation of the fluid.

Two different fluids – water and a water-glycol mixture (40 vol% glycol) – and several different flow rates were tested in the experimentation, the latter of which were quantified through an off-line characterization that measured the quantity of liquid flowing in a container during a defined time period. Some issues related to the production of rust in the collectors and the consequent obstruction of pumps arose during the experimentation (Fig. 4c and d). However, these issues could be solved through the use of stainless-steel collectors and commercially available anti-rust, and anti-frozen products.

During the experimentation, the test room was heated, by means of an electric oil heater, to about 20 °C.

The sub-modules were equipped with several sensors to monitor the following variables: i) the surface, liquid, and air temperatures, by means of calibrated type-T and type-E thermocouples (accuracy varying between  $\pm 0.25$  °C and  $\pm 1.0$  °C); ii) the heat fluxes on the internal surfaces, by means of HFP-01 heat flux meter sensors (sensitivity  $0.015 \mu\text{V}/\text{Wm}^2$ , uncertainty of calibration  $\pm 3\%$ ); iii) the heat fluxes on the MFG cavity surface, by means of MF-180 heat flux meter sensors by Eko (sensitivity  $0.024 \mu\text{V}/\text{Wm}^2$ ); iv) the incident vertical solar radiation ( $I_{\text{inc}}$ ), horizontal global solar radiation ( $I_{\text{hor}}$ ), and the transmitted vertical solar radiation ( $I_{\text{en}}$ ), by means of LP02 pyranometers (sensitivity  $0.013 \div 0.019 \mu\text{V}/\text{Wm}^2$ , uncertainty of calibration  $\pm 1.8\%$ ). These devices were located on the external south façade of the test cell ( $I_{\text{inc}}$ ), on the horizontal surface of the roof ( $I_{\text{hor}}$ ) and facing the internal surface of the transparent component ( $I_{\text{en}}$ ). A schematic representation of the sensors installed on the TGUs is shown in Fig. 5. The temperatures of the MFG and of the internal and external surfaces of the TGUs were measured at three heights in the center and on the sides of the component, while the other layers were monitored at their central points. All the thermocouples inside the TGUs were attached during the construction process of the glazing systems. The inlet and outlet liquid temperatures were measured by means of thermocouples attached to the steel pipes connecting the collectors to the PVC pipes. In the TSMA case, the

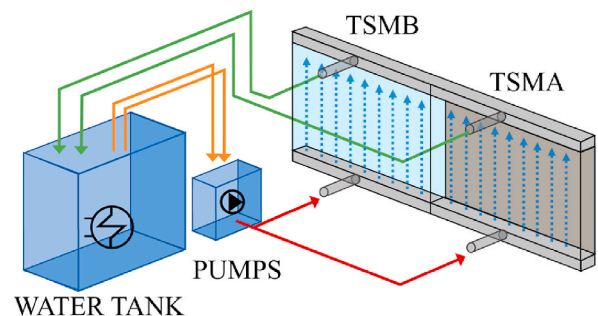


Fig. 3. Scheme of the hydraulic system.

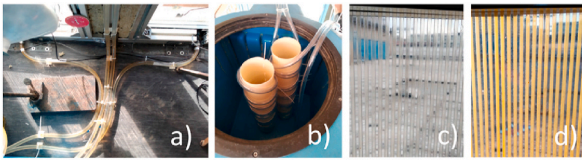


Fig. 4. A) Hydraulic PVC pipe circuit; b) heat exchanger; c) MFG with flowing water; d) MFG with a rust and glycol mixture.

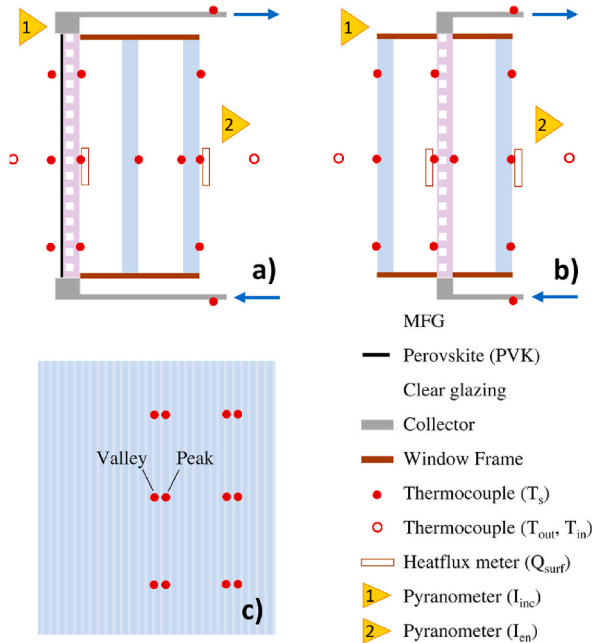


Fig. 5. Scheme of the sensor positions: a) TSMA vertical sections; b) TSMB vertical section; c) TSMA façade.

steel collector was placed externally, due to the structure of the IGU, and insulated with a thin expanded polystyrene (EPS) layer: this determined the presence of a thermal bridge, which in turn resulted in non-negligible heat losses that affected the circulating (inlet and outlet) fluid temperature. A “Datataker DT85” datalogger, connected to a PC, acquired data from all the sensors at a time-step of 5 min.

#### 2.4. Designing the monitoring campaign and data analysis

The monitoring activity was performed in the winter season, from December 2021 to February 2022, and the MFG was operated with different circulating liquids and at different flow rates in order to perform comparative measurements (see Table 1). Measurements with water were performed to obtain reference data.

It was necessary to verify the fluid flow distribution in width and height in the MFG components in order to select appropriate flow rates for the in situ placed prototypes. For this purpose, an infrared thermography of the MFG of TSMA was carried out, using a TESTO 875

Table 1

Flowing solutions, typical days and flow rates assessed in the field.

CASE	LIQUID	Typical day		Flow rate [l/h]	
		TSMA	TSMB	TSMA	TSMB
A	Water	02.Dec	02.Dec	16.5	16.5
B	Water + glycol 40%	13.Feb	13.Feb	0	0
C	Water + glycol 40%	19.Dec	19.Dec	16.5	16.5
D	Water + glycol 40%	15.Jan	15.Jan	27.8	9.3
E	Water + glycol 40%	05.Feb	05.Feb	23.4	24.2

thermal imaging camera, and the external surface was covered with a thin white vinyl layer to avoid any visible or thermal wavelength reflection. The analysis was performed with a circulating water-glycol mixture (see Table 1) at 35 °C, at flow rates of 5.7 l/h, 11.1 l/h, and 35 l/h, respectively (measured over a frontal width of the component of 0.58 m, which is equivalent to 9.8 l/h, 19.1 l/h and 60.3 l/h, respectively, over a frontal width of 1 m).

Typical days characterized by similar solar radiation and external temperature profiles (see Fig. 6) were selected for the data analysis to compare the temperatures and heat flows of the different configurations under the same weather conditions. However, the glazing temperature and heat flow results could have been affected by the differences in the external temperature data (up to 5 °C of difference); it was expected that higher heat flows and lower glazing temperatures would be measured in the colder days, as well as differences in the solar heat gains, depending on the clearness of the sky. Moreover, the use of different power pumps in the modules, due to the different rust status of the collectors, led to different flow rates during the same day and to some uncertainties in their measured values. For this reason, the performance comparison between the two components is provided in the data analysis for the equivalent flow rate.

### 3. Results and discussion

The results of the simulations and of the experimental monitoring are presented and discussed in this section.

#### 3.1. Designing the IGUs with Window7.7

The IGUs designed with Window7.7 were analyzed, in terms of surface temperature,  $U_{\text{value}}$ ,  $g_{\text{value}}$  and  $T_{\text{vis}}$ . The glazing temperature profiles, calculated for CEN summer conditions ( $I_{\text{inc}} = 500 \text{ W/m}^2$ ,  $T_{\text{out}} = 30 \text{ °C}$ ,  $T_{\text{in}} = 25 \text{ °C}$ , external heat transfer coefficient  $h_e = 8 \text{ W/m}^2\text{K}$ , internal heat transfer coefficient  $h_i = 2.5 \text{ W/m}^2\text{K}$ ) are shown in Fig. 7a and b for the different configurations presented in Fig. 1. Fig. 7a shows the results of the IGUs with an external MFG: the maximum temperatures of the MFGs are reached when a PVK layer is present, because of the higher absorbance of the external layer. TGU 5 B is the module that maximizes the external surface temperature, while maintaining the best thermal performance, in terms of  $U_{\text{value}}$  (see Table 2). Fig. 7b presents the results of the TGUs with a central MFG: the highest temperature in the MFG is reached for TGU 5C, in which the external glazing is laminated with PVK and there is just one low-e coating on face 5. However, this configuration, like TGU 5D, has an external PVK layer that is not

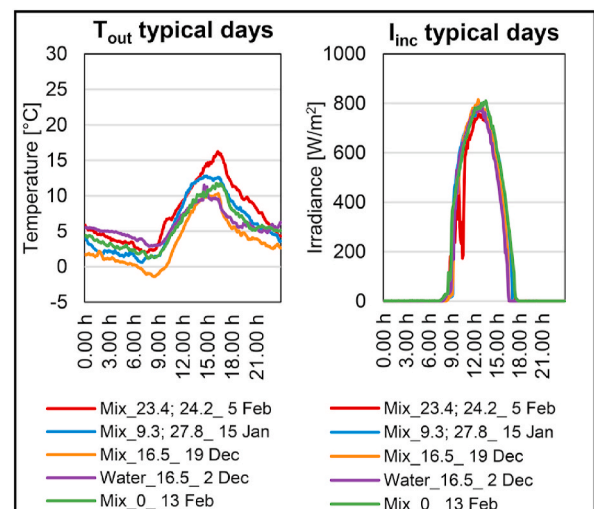


Fig. 6. Irradiance and temperature profiles of the selected days.

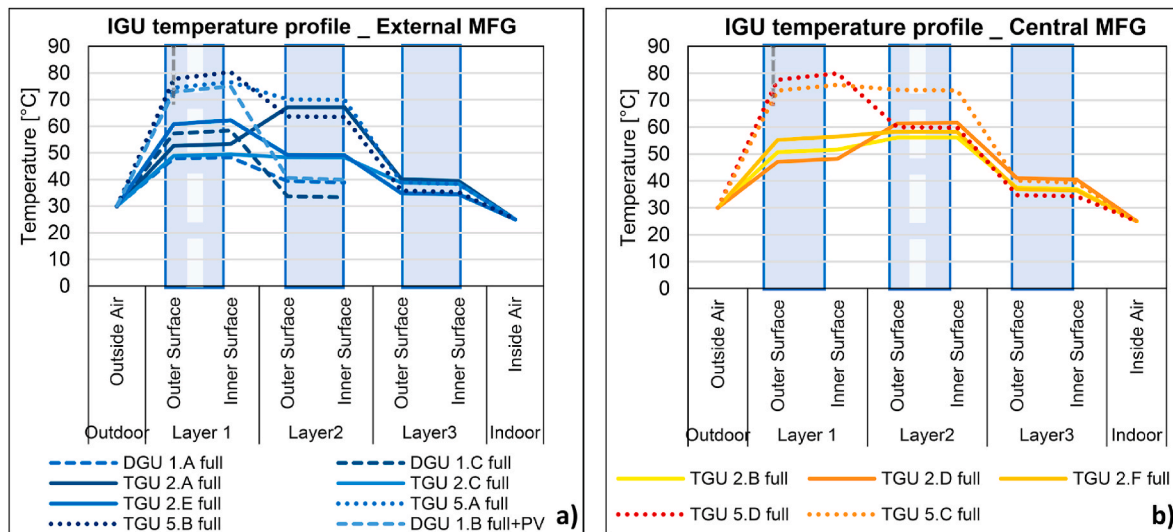


Fig. 7. Surface temperature of the IGUs with a) an external MFG; b) a central MFG.

Table 2

Thermal and visual properties of the analyzed IGUs.

IGU	$U_{\text{value}}$	$g_{\text{value}}$	$T_{\text{vis}}$
DGU 1.A	1.29	0.45	0.61
DGU 1.B + PV	1.27	0.21	0.06
DGU 1.C	1.26	0.36	0.59
TGU 2.A	0.62	0.36	0.49
TGU 2.B	<b>0.71</b>	<b>0.33</b>	<b>0.49</b>
TGU 2.C	0.95	0.42	0.57
TGU 2.D	0.94	0.44	0.56
TGU 2.E	0.61	0.30	0.48
TGU 2.F	0.60	0.30	0.41
TGU 5.A + PV	0.94	0.19	0.06
TGU 5.B + PV	<b>0.62</b>	<b>0.13</b>	<b>0.05</b>
TGU 5.C + PV	0.94	0.20	0.06
TGU 5.D + PV	0.61	0.12	0.05

cooled by the liquid circulating in the MFG and it therefore suffers from some overheating problems; it in fact reached a temperature of 80 °C. The MFG temperatures of the other IGUs are comparable, with TGU 2 B showing the best visual and thermal properties ( $g_{\text{value}} < 0.35$ ,  $T_{\text{vis}} \approx 0.5$ ,  $U_{\text{value}} = 0.71$ ; see Table 2). Configurations TGU 5 B and TGU 2 B were selected, on the basis of the simulation results, for the fabrication and experimental assessment of a prototype under realistic operating conditions.

### 3.2. Thermography

The first step of the experimental campaign involved the verification of the homogeneous flow in all the MFG channels for the different tested flow rates. The thermal images and the temperature distribution over three axes (P1, P2 and P3) are shown in Fig. 8 for the three investigated flow rates. The graphs show the temperature variations across three selected horizontal lines, which are depicted in the images above. The test results demonstrate that a flow rate of 5.7 l/h cannot provide a homogeneous distribution of the temperature in the horizontal direction at different heights. An increased flow rate of 11.1 l/h reduces this inhomogeneity, especially in the lower and upper parts of the component. A flow rate of 35 l/h provides a homogeneous temperature distribution, but simultaneously results in a reduced temperature difference in the vertical direction. Therefore, an appropriate flow rate was identified and tested in the 11.1 l/h to 35 l/h range for this component dimension. These flow rates correspond to flows of 19.1 l/h and 60.3 l/h per m of active length, respectively; the range of 11.4 ÷ 22.9 l/(h m) (40 ÷ 80

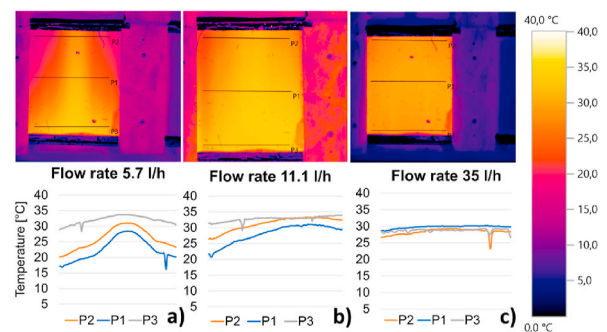


Fig. 8. Thermal images and temperature distribution of three heights with a) 5.7 l/h b) 11.1 l/h c) 35 l/h.

ml/min on 210 mm active length) was previously reported for laboratory studies or small-scale prototypes [13]. The different flow rates in the 11 ÷ 35 l/h range (with an outlier of 9.3 l/h) shown in Table 1 were therefore monitored in situ on the basis of the thermography results.

### 3.3. Glazing temperature trends

The temperature profiles were experimentally evaluated across the IGUs for days with similar boundary conditions and for each configuration (see Fig. 6). The temperatures were determined at the center of each glazing element three different times, at an interval of 3 h: i) a morning timestep: 9:45 a.m.,  $I_{\text{inc}} = 462 \pm 47 \text{ W/m}^2$ ; ii) the peak of irradiance of the day: 12:45 p.m.,  $I_{\text{inc}} = 772 \pm 20 \text{ W/m}^2$ ; iii) an afternoon timestep: 3:45 p.m.,  $I_{\text{inc}} = 446 \pm 35 \text{ W/m}^2$ . As can be seen in Fig. 9a and d, the temperature profiles in the morning are similar for all the configurations and mock-ups. The circulating liquid temperature, which varies between 12.1 °C and 18.5 °C at the TSMA inlet, and between 13.4 °C and 15.6 °C at the TSMB inlet, does not have a noticeable influence on the temperature of the MFG. The temperature profiles monitored at 12:45 p.m. are presented in Fig. 9b and e. Significant differences in the surface temperature of the MFG can be observed between the configurations with non-circulating and circulating liquids. In fact, the temperatures recorded on the external surface (surface 1, next to the PVK layer) for TSMA is about 9.5 °C lower than when the liquid is circulating inside the capillaries of the MFG. An even higher temperature difference was recorded in the 23.8 ÷ 25.6 °C range between the configurations with non-circulating and circulating liquids on the



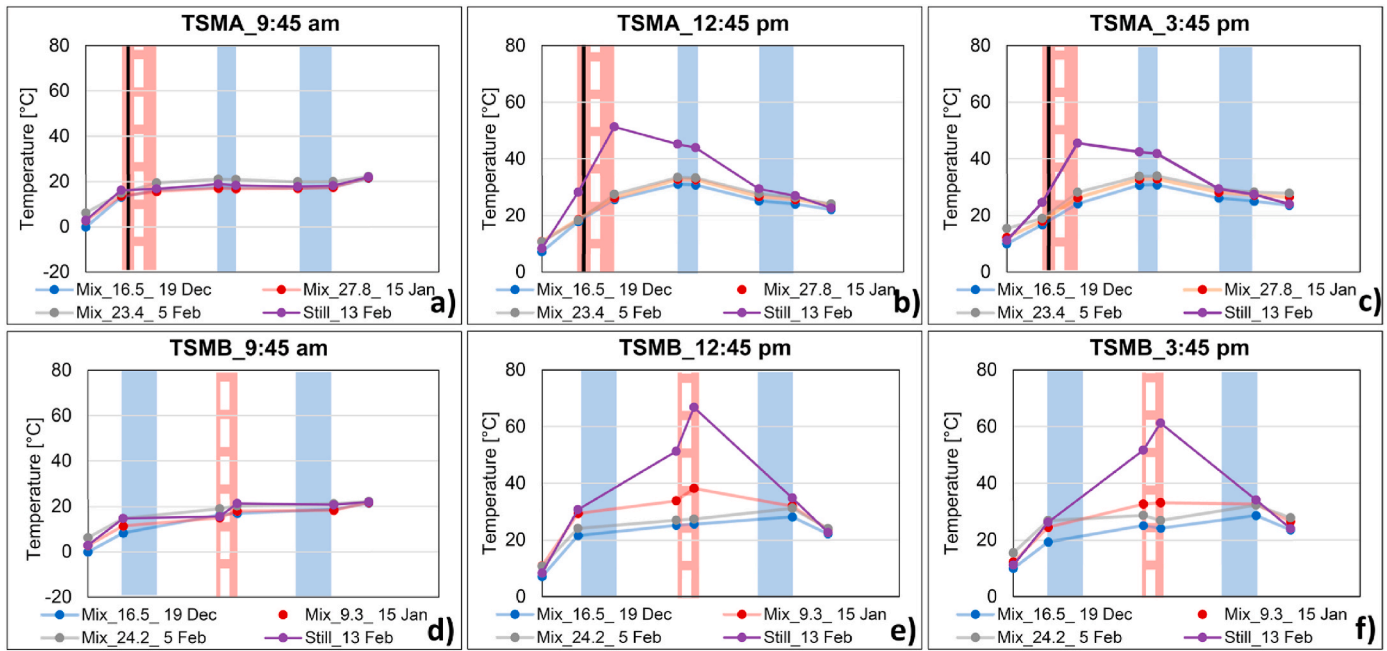


Fig. 9. Temperature profiles of TSMA and TSMB at a) 9:45 a.m.; b) 12:45 p.m.; c) 3:45 p.m.

surface of the MFG facing the cavity (surface 2). The temperature difference in the central panel decreases to about  $11.8 \div 14.1$  °C for surface 3, and to about  $10.7 \div 13.1$  °C for surface 4. No significant differences are observable for the internal panel between the configurations with non-circulating and circulating fluids. Comparable results are obtained for the third timestep, that is, at 3:30 p.m. (Fig. 9c): the glazing temperatures are reduced by  $5.6 \div 7.9$  °C (surface 1),  $17.3 \div 21.4$  °C (surface 2),  $8.6 \div 11.7$  °C (surface 3), and  $7.9 \div 10.9$  °C (surface 4), respectively, under circulating fluid conditions. The MFG with a circulating fluid is therefore effective in reducing the temperatures of the different layers, and the differences in the temperatures between the flow rates could be imputable to slightly different boundary conditions and require further investigation.

The temperature differences in the  $1.3 \div 9.2$  °C (surface 1),  $17.5 \div 26.1$  °C (covering glass of the MFG, surface 3), and  $28.6 \div 41.2$  °C (capillary glass of MFG, surface 4) ranges for TSMB, at 12:45 p.m. (Fig. 9e) were determined for the non-circulating and circulating liquid conditions. The temperature differences on the internal surface reduced to about  $2.2 \div 6.6$  °C. Operation of the MFG is highly effective in lowering the glazing temperature in this configuration, and the differences in the performance that depend on the flow rate of the circulating liquid can easily be identified. The surface temperature of the covering glass of the MFG decreased by about 10 °C when the flow rate was increased from 9.3 l/h to 24 l/h. The results obtained at 3:30 p.m., which were similar to those of TSMA, were comparable to the trends of the temperature differences recorded at 12:45 (Fig. 9f), i.e.,  $1.7 \div 6.9$  °C (surface 1),  $19.0 \div 26.5$  °C (surface 3),  $28.0 \div 37.1$  °C (surface 4), and  $1.4 \div 5.5$  °C (surface 6), respectively. The MFG in this configuration can also reduce the internal surface temperature, thereby contributing to an improved indoor thermal comfort when such a configuration is installed in buildings.

The difference in the MFG temperature between the top and bottom daily profiles for different flow rates is shown in Fig. 10. It can be seen that the higher the flow rate is, the smaller the temperature difference between the top and bottom, with a maximum of 12.2 °C in TSMA and 6.6 °C in TSMB, respectively. A flow rate of 24 l/h is able to flatten the MFG temperature difference in TSMB, while a flow rate of 27.8 l/h still causes a gradient of about 7.8 °C in TSMA.

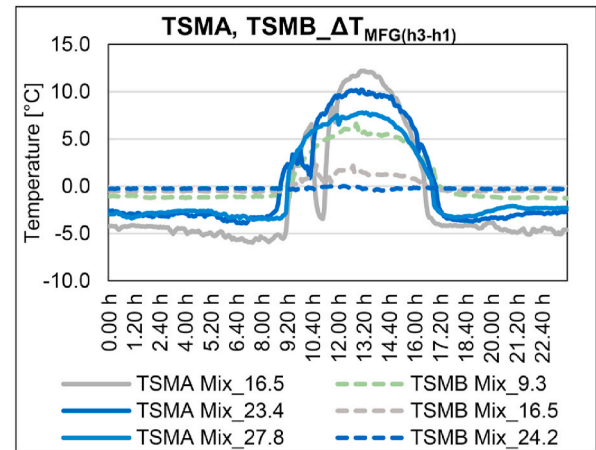


Fig. 10. Temperature difference in MFG between the top and bottom daily profiles.

### 3.4. Outlet-inlet temperature difference

The fluid outlet-inlet temperature differences ( $\Delta T_{\text{outlet-inlet, exp}}$ ) measured in the two sub-modules are presented hereafter. These results may be affected by heat conduction through the steel collector phenomena, the magnitude of which is as yet unknown. Fig. 11 shows the  $\Delta T_{\text{outlet-inlet, exp}}$  daily profile for different configurations, which is negative for almost all the nighttime cases, with a maximum temperature difference of up to  $-4.1$  °C, and positive in the daytime. Fig. 12 shows the corresponding fluid outlet temperature ( $T_{\text{outlet}}$ ) profiles. The peak temperatures at the outlet vary between  $29.2$  and  $33.1$  °C for TSMA, and between  $25.1$  and  $35.1$  °C for TSMB. The water tank temperature varies over the considered time interval between  $15.3 \div 21.9$  °C. The peak values and 95 percentiles of the fluid temperature differences are shown in Fig. 13. The 95 percentiles of  $\Delta T_{\text{outlet-inlet, exp}}$  are  $15.6$  °C (16.5 l/h flow rate),  $4.0$  °C (23.4 l/h flow rate), and  $4.4$  °C (27.8 l/h flow rate), respectively, for TSMA. A reduced flow rate thus maximizes the heat collection of the fluid.

The 95 percentiles of  $\Delta T_{\text{outlet-inlet, exp}}$  are  $11.3$  °C (9.3 l/h flow rate),

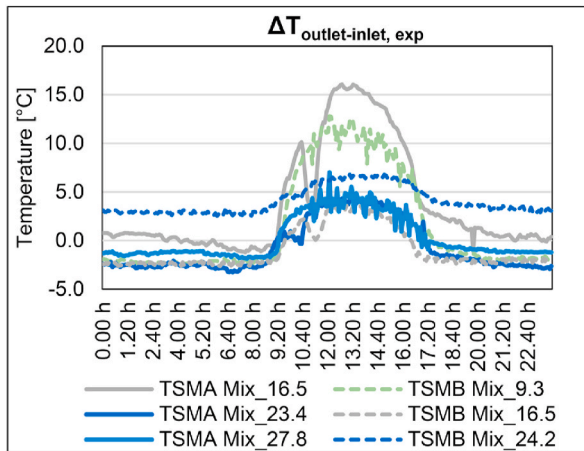


Fig. 11. The  $\Delta T_{out, in, exp}$  daily profile for different configurations.

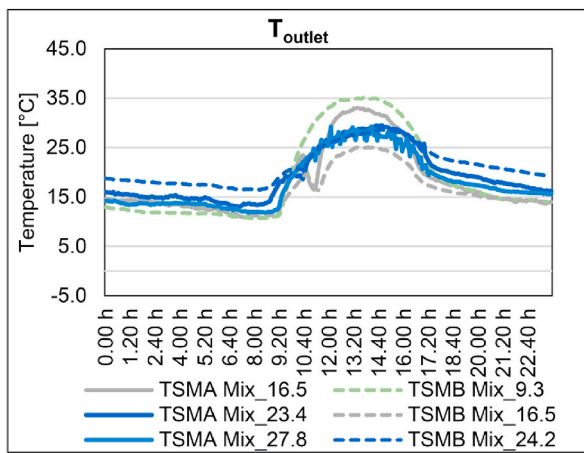


Fig. 12. The  $T_{outlet}$  daily profile for different configurations.

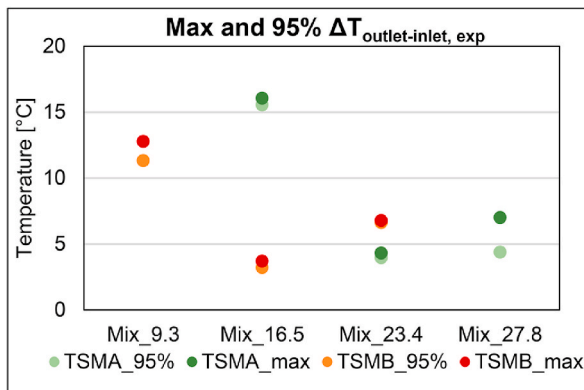


Fig. 13. Peak values of the 95 percentiles of  $\Delta T_{out, in, exp}$  for different configurations.

3.2 °C (16.5 l/h flow rate), and 6.6 °C (24 l/h flow rate), respectively, for TSMB. Again, a reduced flow rate contributes to an increase in  $\Delta T_{outlet-inlet, exp}$ . The results demonstrate the importance of appropriate adjustments to the flow rate in order to obtain a homogeneous flow in the MFG together with a maximum heat harvesting efficiency.

### 3.5. Heat flows

Two heat flux meters, placed on the internal surface of the two prototypes, were used to measure the total heat exchange between the glass surface and the internal environment ( $Q_{surf}$ ). The results are shown in Fig. 14. The highest heat flows in each sub-module, in terms of heat gain (during the day) and loss (during the night), were measured when the MFG was operated under non-circulating conditions. These results further indicate an important influence of the absorbance of the IGU and the position of the MFG on the heat transfer through the glazing and, consequently, on the heat recovered by the circulating liquid. Figs. 15 and 16 show the integrated daily values of the positive and negative heat flows for the investigated configurations: the introduction of a circulating liquid in TSMA leads to a reduction in the daily heat gains over the 50 ÷ 71% range, which depends on the flow rate, whereas the night losses are reduced by about 50 ÷ 85%. A higher flow rate results in an increased daily heat flow. The daily heat gains for TSMB are reduced by about 30 ÷ 41%, whereas the night losses are reduced by about 73 ÷ 87%. No obvious influence of the flow rate can be seen for this configuration.

### 3.6. Assessment of the thermal and solar performance of the experimental KPIs

The  $U_{value, exp}$ ,  $g_{value, exp}$  and  $T_{sol, exp}$  of the two installed prototypes were assessed in situ using the methodology presented in Section 2.1. The solar transmission, discretized on the basis of the solar angle, of the two TGUs calculated in different periods of the experimental campaign is presented in Fig. 17. As can be seen from the results, the properties of the TSMB sub-module were affected by variations in the optical and thermal properties, as a result of the presence of rust and blue glycol, while the properties of TSMA, which is characterized by a very low visible transmission, remained almost unvaried due to the presence of the highly-absorptive external PVK layer. The experimental thermal transmittance of the components under different conditions and their absolute errors calculated by means of the propagation of uncertainty method are shown in Fig. 18. Table 3 shows the  $U_{value, exp}$  and  $g_{value, exp}$  with their calculated absolute error. The experimentally determined values of  $U_{value, exp}$  in the absence of a flowing liquid, are consistently lower than the values of  $U_{value}$  simulated by Window7.7 under standard conditions (from 0.71 W/m<sup>2</sup>K to 0.65 W/m<sup>2</sup>K for TSMB and from 0.62 W/m<sup>2</sup>K to 0.54 W/m<sup>2</sup>K for TSMA). The presence of a non-circulating (still) water-glycol mixture further reduces the magnitude of  $U_{value, exp}$ . When the liquid inside the component is circulating at a rate of 16.5 l/h, the  $U_{value, exp}$  decreases to 0.13 W/m<sup>2</sup>K for TSMA and to 0.15 W/m<sup>2</sup>K for

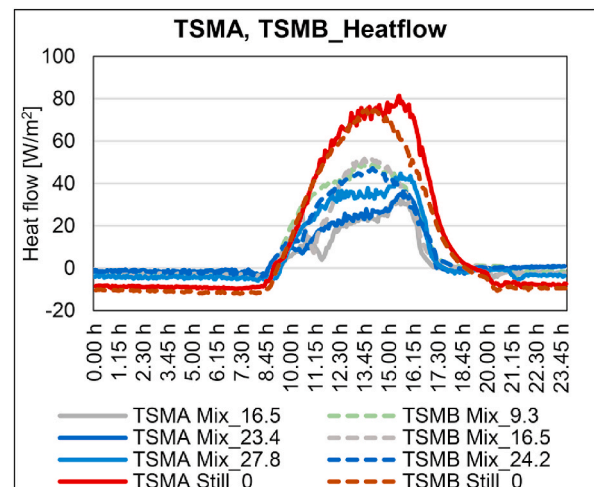


Fig. 14.  $Q_{surf}$  for different configurations and IGUs.



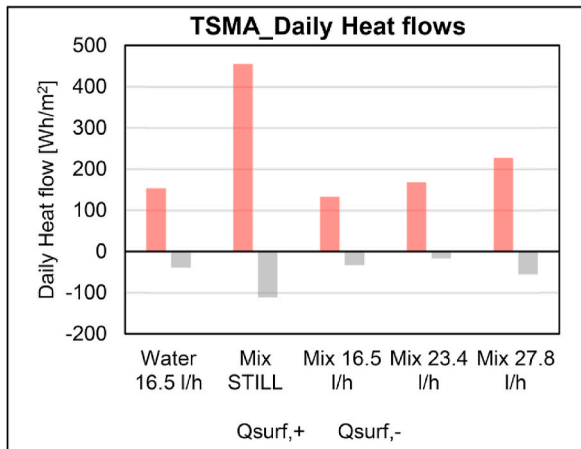


Fig. 15. Positive and negative integrated daily values of the TSMA heat flows.

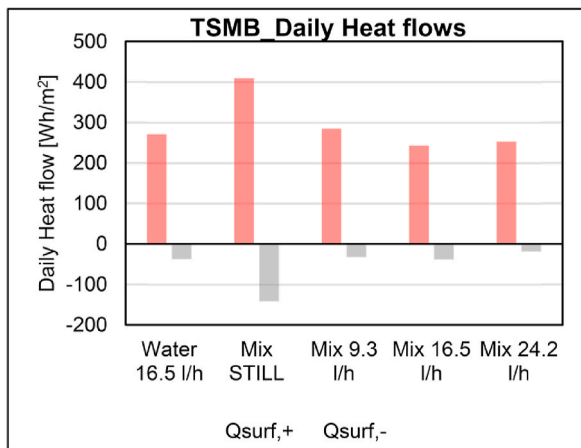


Fig. 16. Positive and negative integrated daily values of the TSMB heat flows.

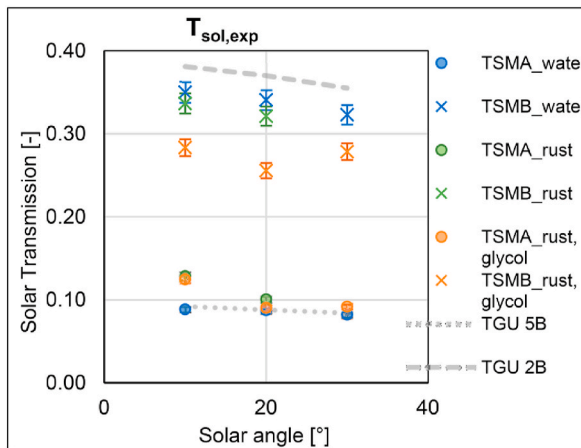


Fig. 17. Solar transmission discretized by the angle.

TSMB, with a reduction of around 70%. However, this value does not take into account the contribution of the water, which is cooled and introduced into the environment during the night period. An increase in the flow rate to 24 l/h results in a further decrease in  $U_{value,exp}$  from 0.13 W/m<sup>2</sup>K to 0.07 W/m<sup>2</sup>K for TSMA and from 0.15 W/m<sup>2</sup>K to 0.11 W/m<sup>2</sup>K for TSMB. These experimental results show that the MFG effectively improves the thermal performance of the transparent component itself;

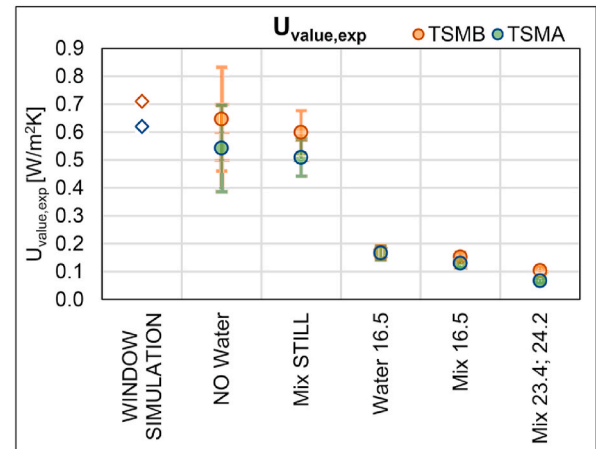


Fig. 18. Experimental thermal transmittance for different set-up conditions.

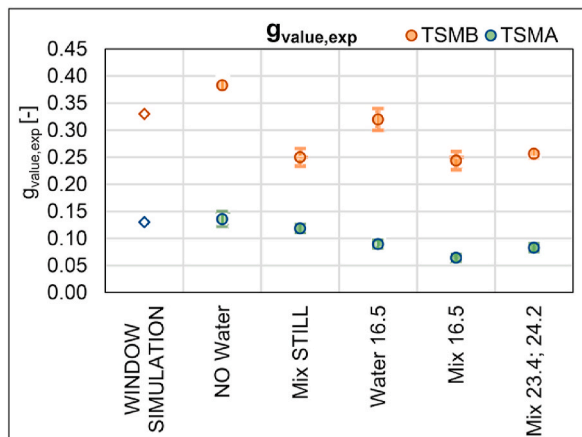
however, appropriate KPIs that can take into account the heat transfer through the flowing liquid still need to be identified and calculated, taking into consideration the fluid source and use (i.e. water supply network or tank, heat storage, passive cooling, or other uses). The results of the experimentally determined solar heat gain coefficients are shown in Fig. 19. The simulated TSMA  $g_{value}$  matches the one measured in the absence of liquid and with a non-circulating water-glycol mixture. The presence of a circulating water-glycol mixture lowers  $g_{value,exp}$  from 0.12 to 0.06 (flow rate of 16.5 l/h) and 0.08 (flow rate of 24 l/h), depending on the flow rate. The discrepancy in the  $g_{value,exp}$  reduction depends on the different boundary conditions in which the KPI have been calculated (17th-21st December; 4th-9th February). This suggests the need to organize a dense schedule to avoid disparity in the measurements as much as possible. The  $g_{value,exp}$  in the absence of water results to be higher for TSMB than the simulated one (0.38 vs 0.33), while it results to be equal to 0.25 in the presence of a non-circulating water-glycol mixture. Circulation of the fluid lowers the value from 0.25 to 0.24 (water-glycol mixture, flow rate of 16.5 l/h). A higher flow rate (water-glycol mixture, and a flow rate of 23.8 l/h) results in a higher  $g_{value,exp}$ , which is equal to 0.26: this is due to the greater contribution of the transmitted solar irradiance,  $I_{en}$ , due to the external boundary conditions. The same occurs for the measured  $g_{value,exp}$  with water flowing at 16.5 l/h, which is equal to 0.32, due to the higher solar transmittance of the transparent flowing liquid. This transparent component shows a limited efficacy in controlling solar heat gains, which depends more on the transmitted irradiance contribution than the secondary heat flux one.

#### 4. Conclusions and future works

The present paper describes the results of an experimental campaign set up to assess the energy performance of MFG components in a real application. The methodology followed in the design of the experimental campaign started with the identification of the KPIs and a preliminary steady-state simulation to identify appropriate IGU configurations to be tested in the field. Two small TGUs that integrate MFGs and PVK were mounted and tested while varying the liquid flow rate during the winter season in an outdoor test cell located on the roof of the Politecnico di Torino, Italy. The preliminary results pertaining to the surface and fluid temperatures, heat flows, and temperature distribution under different test conditions, including different circulating fluids and flow rates, are presented herein. The simulation results have demonstrated that the position of MFG in an IGU and the absorbance of the layer to which it is coupled are two relevant factors that influence the energy performance of the component, and they therefore have to be designed carefully, according to the objectives of the component. In

**Table 3**Experimental KPIs:  $U_{\text{value,exp}}$  with absolute error.

CASE	$U_{\text{value,exp}}$ [ $\text{W}/\text{m}^2\text{K}$ ]		$U_{\text{value,exp}}$ AERR [ $\text{W}/\text{m}^2\text{K}$ ]		$g_{\text{value,exp}}$ [–]		$g_{\text{value,exp}}$ AERR [–]	
	TSMA	TSMB	TSMA	TSMB	TSMA	TSMB	TSMA	TSMB
Window 7.7	0.62	0.71	–	–	0.13	0.33	–	–
NO Water	0.54	0.65	$\pm 0.16$	$\pm 0.19$	0.14	0.38	$\pm 0.01$	$\pm 0.03$
Mix, STILL	0.51	0.6	$\pm 0.07$	$\pm 0.08$	0.12	0.25	$\pm 0.01$	$\pm 0.02$
Water, 16.5 l/h	0.17	0.17	$\pm 0.02$	$\pm 0.02$	0.09	0.32	$\pm 0.01$	$\pm 0.02$
Mix, 16.5 l/h	0.13	0.15	$\pm 0.02$	$\pm 0.02$	0.06	0.24	$\pm 0.01$	$\pm 0.02$
Mix, 23.4; 24.2 l/h	0.07	0.11	$\pm 0.01$	$\pm 0.01$	0.08	0.26	$\pm 0.01$	$\pm 0.02$

**Fig. 19.** Experimental solar heat gain coefficient for different set-up conditions.

In addition, the results allowed the prototype configurations and set-up conditions to be selected, in terms of layer coupling, circulating liquid, and the applied flow rates to be tested in situ. The experimental campaign also provided some practical insights concerning the choice of the colour of the liquid mixture and its influence on the performance of the components. Moreover, it allowed particular attention to be paid to the power and prevalence of the pump and to the design of the hydraulic circuit, as well as to the caution needed when monitoring the liquid temperature and solving the problem of thermal bridges in the presence of steel collectors on the façade. The experimental results showed that MFG is effective in reducing the surface temperature (by as much as  $10.4\text{ }^{\circ}\text{C}$  in the PV layer) and maintaining the efficiency of PV when coupled with Perovskite. Moreover, MFG is very effective in reducing the temperature of the TGU layers when used as a central panel and has shown the potential to reduce the thermal stress of the glazing layers. The MFG temperature reduction on the internal surface (as much as  $6.6\text{ }^{\circ}\text{C}$  for the TGU with a central MFG) can help reduce thermal discomfort, due to the contribution of the radiative surface, without affecting the solar and visible transmittance of the component, even though the module with the PV layer results in very low values of both, as it is unsuitable for transparent applications.

In terms of heat flows, the MFG is effective in decreasing the heat transfer through the component during the day and night, with a percentage that varies between 30% and 71%, depending on the TGU configuration and on the flow rate. This result is in agreement with the experimentally assessed thermal transmittance reduction obtained for during the night. However, the modulation of the solar heat gain coefficient was not effective in the monitored transparent component and resulted in a low efficacy of the summer thermal performance, while a variation of up to 46% was observed for the value of the PV integrated module.

Considering the energy harvesting capabilities of the MFG, an increase in temperature of the circulating liquid between the inlet and outlet of up to  $12\text{--}16\text{ }^{\circ}\text{C}$  was determined, a value that depended on the

position of the MFG and on the properties of the glazing layers. However, the use of the warm fluid ( $T_{\text{outlet}} = 23\text{--}32\text{ }^{\circ}\text{C}$ ) produced by the MFG still has to be investigated and designed in combination with other technologies (PV, PCM). The complexity of the technology has to be taken into consideration carefully and compared with the obtained benefits. Moreover, a Life Cycle Cost Analysis is necessary to understand the production, design, and operation costs of the technology, as well as the return of investment in a real-world application to obtain a comprehensive evaluation of the efficiency of this technology.

The future works on this topic will involve installing and monitoring a full mock-up of one of the tested prototypes in a long-term experimental campaign, in which the methodology provided in this study will be followed and expanded. Novel KPIs will be identified for the assessment of the thermal behavior of the components and simplified models of the MFG technology will be developed and validated by resorting to the collected data. This will allow a building-scale model to be developed and used to analyze the performance of the overall technology, as well as to establish the possible building-level energy savings.

### Credit author statement

Manuela Baracani: Methodology, Formal analysis, Investigation, Writing – original draft, Writing – review & editing, Visualization. Fabio Favoino: Conceptualization, Methodology, Writing – review & editing, Supervision. Stefano Fantucci: Conceptualization, Methodology Writing – original draft, Writing – review & editing, Supervision, Project administration, Funding acquisition. Valentina Serra: Writing – original draft, Writing – review & editing, Supervision, Project administration, Funding acquisition. Marco Perino: Supervision, Project administration, Funding acquisition. Marisandra Introna: Formal analysis, Investigation, Visualization. Rene Limbach: Data curation, Resources, Writing – review & editing. Lothar Wondraczek: Conceptualization, Data curation, Resources, Writing – review & editing.

### Declaration of competing interest

The authors declare that they have no known competing financial interests or personal relationships that could have appeared to influence the work reported in this paper.

### Data availability

The data that has been used is confidential.

### Acknowledgment

The POWERSKIN PLUS project has received funding from the European Union's Horizon 2020 research and innovation program under Grant Agreement No. 869898.

The authors wish to thank Roman Sajzew from the Otto Schott Institute of Materials Research, Friedrich Schiller from the University of Jena, Germany, for conducting the optical spectroscopic analyses, and the Flachglas Gruppe (FGS) for providing the mock-up glasses. The

support of Michela di Renna during the experimental campaign is gratefully acknowledged.

## References

- [1] Economidou M, Todeschi V, Bertoldi P, D'Agostino D, Zangheri P, Castellazzi L. Review of 50 years of EU energy efficiency policies for buildings. *Energy Build* 2020;225:110322. <https://doi.org/10.1016/j.enbuild.2020.110322>.
- [2] E.orts. The Department of Energy's Renewable Energy; 2012. <https://www.energy.gov/>. [Accessed 28 April 2022].
- [3] IEA. Transition to Sustainable Buildings - Analysis. <https://www.iea.org/reports/transition-to-sustainable-%0Abuildings> (accessed March. 15, 2023).
- [4] Baetens R, Jelle BP, Gustavsen A. Properties, requirements and possibilities of smart windows for dynamic daylight and solar energy control in buildings: a state-of-the-art review. *Sol Energy Mater Sol Cells* 2010;94(2):87–105. <https://doi.org/10.1016/j.solmat.2009.08.021>.
- [5] Chow T, Li C, Lin Z. Innovative solar windows for cooling-demand climate. *Sol Energy Mater Sol Cells* 2010;94(2):212–20. <https://doi.org/10.1016/j.solmat.2009.09.004>.
- [6] Sierra P, Hernández JA. Solar heat gain coefficient of water flow glazings. *Energy Build* 2017;139:133–45. <https://doi.org/10.1016/j.enbuild.2017.01.032>.
- [7] Chow T-T, Li C, Lin Z. Thermal characteristics of water-flow double-pane window. *Int J Therm Sci* 2011;50(2):140–8. <https://doi.org/10.1016/j.ijthermalsci.2010.10.006>.
- [8] Hale GM, Querry MR. Optical constants of water in the 200-nm to 200- $\mu$ m wavelength region. *Appl Opt* 1973;12(3):555. <https://doi.org/10.1364/AO.12.000555>.
- [9] Gutai M, Kheybari AG. Energy consumption of water-filled glass (WFG) hybrid building envelope. *Energy Build* 2020;218:110050. <https://doi.org/10.1016/j.enbuild.2020.110050>.
- [10] Chow TT, Lyu Y. Effect of design configurations on water flow window performance. *Sol Energy* 2017;155:354–62. <https://doi.org/10.1016/j.solener.2017.06.050>.
- [11] Chow T-T, Lyu Y. Numerical analysis on the advantage of using PCM heat exchanger in liquid-flow window. *Appl Therm Eng* 2017;125:1218–27. <https://doi.org/10.1016/j.applthermaleng.2017.07.098>.
- [12] Yamaç Hİ, Koca A. Investigation of water flow window with/without energy storage tank during winter season. *Appl Therm Eng* 2023;225:120164. <https://doi.org/10.1016/j.applthermaleng.2023.120164>.
- [13] Heiz BPV, Pan Z, Lautenschläger G, Sirtl C, Kraus M, Wondraczek L. Ultrathin fluidic laminates for large-area façade integration and smart windows. *Adv Sci* 2017;4(3):1600362. <https://doi.org/10.1002/advs.201600362>.
- [14] Heiz B, Pan Z, Wondraczek L. Outdoor performance of fluidic glass–glass laminate windows for building integration. *Energy Technol* 2019;7. <https://doi.org/10.1002/ente.201800810>.
- [15] Su L, Fraaß M, Kloas M, Wondraczek L. Performance analysis of multi-purpose fluidic windows based on structured glass-glass laminates in a triple glazing. *Front. Mater.* 2019;6. <https://doi.org/10.3389/fmats.2019.00102>.
- [16] Heiz B, Pan Z, Su L, Si Le T, Wondraczek L. A large-area smart window with tunable shading and solar-thermal harvesting ability based on remote switching of a magneto-active liquid. *Adv. Sustain. Syst.* 2018;2. <https://doi.org/10.1002/adssu.201700140>.
- [17] V Heiz BP, Su L, Pan Z, Wondraczek L. Fluid-integrated glass – glass laminate for sustainable hydronic cooling and indoor air conditioning, vol. 1800047; 2018. p. 1–8. <https://doi.org/10.1002/adssu.201800047>.
- [18] Su L, Fraaß M, Wondraczek L. Design guidelines for thermal comfort and energy consumption of triple glazed fluidic windows on building level. *Adv. Sustain. Syst.* 2021;5(2):2000194. <https://doi.org/10.1002/adssu.202000194>.
- [19] Rockendorf G, Janssen S, Felten H. Transparently insulated hybrid wall. *Sol Energy* 1996;58(1–3):33–8. [https://doi.org/10.1016/0038-092X\(96\)00044-8](https://doi.org/10.1016/0038-092X(96)00044-8).
- [20] Zhang C, Ji J, Wang C, Ke W, Xie H, Yu B. Experimental and numerical studies on the thermal and electrical performance of a CdTe ventilated window integrated with vacuum glazing. *Energy* 2022;244:123128. <https://doi.org/10.1016/j.energy.2022.123128>.
- [21] Wen X, Ji J, Song Z. Performance comparison of two micro-channel heat pipe LFPV/T systems plus thermoelectric generators with and without aerogel glazing. *Energy* 2021;229:120704. <https://doi.org/10.1016/j.energy.2021.120704>.
- [22] Kumar NS, Babu KC. A review on perovskite solar cells (PSCs), materials and applications. *J Mater* 2021;7(5):940–56. <https://doi.org/10.1016/j.jmat.2021.04.002>.
- [23] Powerskin+ WALLS ENERGIZING BUILDINGS. <https://www.powerskinplus.eu/>. [Accessed 2 January 2023].
- [24] Attia S, Bilir S, Safy T, Struck C, Loonen R, Goia F. Current trends and future challenges in the performance assessment of adaptive façade systems. *Energy Build* Nov. 2018;179:165–82. <https://doi.org/10.1016/j.enbuild.2018.09.017>.
- [25] Favoino F, Goia F, Perino M, Serra V. Experimental analysis of the energy performance of an ACTIVE , RESponsive and Solar (ACTRESS) facade module. *Sol Energy* 2020;133(2016):226–48. <https://doi.org/10.1016/j.solener.2016.03.044>.
- [26] Building components and building elements - thermal resistance and thermal transmittance - calculation methods (ISO 6946:2017). 2007.
- [27] OPTICS6. <http://windows.lbl.gov/software/optics>.
- [28] WINDOW7.7. <http://windows.lbl.gov/software/window>.